Biochemical and Biophysical Research Communications 444 (2014) 171–176

Contents lists available at ScienceDirect

Biochemical and Biophysical Research Communications

journal homepage: www.elsevier.com/locate/ybbrc

Astrocytic gap junctional networks suppress cellular damage in an *in vitro* model of ischemia

Takanori Shinotsuka, Masato Yasui, Mutsuo Nuriya *

Department of Pharmacology, School of Medicine, Keio University, 35 Shinanomachi, Shinjuku, Tokyo 160-8582, Japan

ARTICLE INFO

Article history:
Received 26 December 2013
Available online 16 January 2014

Keywords:
Calcium
Astrocyte
Gap junction
Two-photon microscopy
Anoxic depolarization

ABSTRACT

Astrocytes play pivotal roles in both the physiology and the pathophysiology of the brain. They communicate with each other via extracellular messengers as well as through gap junctions, which may exacerbate or protect against pathological processes in the brain. However, their roles during the acute phase of ischemia and the underlying cellular mechanisms remain largely unknown. To address this issue, we imaged changes in the intracellular calcium concentration ($[Ca^{2+}]_i$) in astrocytes in mouse cortical slices under oxygen/glucose deprivation (OGD) condition using two-photon microscopy. Under OGD, astrocytes showed $[Ca^{2+}]_i$ oscillations followed by larger and sustained $[Ca^{2+}]_i$ increases. While the pharmacological blockades of astrocytic receptors for glutamate and ATP had no effect, the inhibitions of gap junctional intercellular coupling between astrocytes significantly advanced the onset of the sustained $[Ca^{2+}]_i$ increase after OGD exposure. Interestingly, the simultaneous recording of the neuronal membrane potential revealed that the onset of the sustained $[Ca^{2+}]_i$ increase in astrocytes was synchronized with the appearance of neuronal anoxic depolarization. Furthermore, the blockade of gap junctional coupling resulted in a concurrent faster appearance of neuronal depolarizations, which remain synchronized with the sustained $[Ca^{2+}]_i$ increase in astrocytes. These results indicate that astrocytes delay the appearance of the pathological responses of astrocytes and neurons through their gap junction-mediated intercellular network under OGD. Thus, astrocytic gap junctional networks provide protection against tissue damage during the acute phase of ischemia.

1. Introduction

Ischemia causes cellular damages within minutes and leads to severe brain dysfunctions [1]. Clinically, therapeutic treatments should be started during the early stage of ischemia to prevent brain dysfunction. Therefore, an understanding of the pathophysiology of the acute phase of ischemia is essential for developing an effective treatment strategy for reducing post-ischemic brain damage. Morphological and functional interactions of astrocytes with both neurons and blood vessels suggest that astrocytes play key roles in the pathophysiological processes of ischemia [2]. In response to ischemic insults, several pathophysiological changes have been reported in astrocytes as well as in neurons, such as increases in the intracellular calcium concentration ($[Ca^{2+}]_i$) [3–5], depolarization of the membrane potential [6], cell swelling [7] and a leaky blood–brain barrier at their endfeet [8]. However, whether astrocytes exacerbate or protect against ischemic insults during the acute phase remains unclear [2,9].

Astrocytes communicate with other cells via two major mechanisms: (1) extracellular transmissions via neurotransmitters or gliotransmitters, and (2) intercellular connections via gap junctions [10,11]. As for the extracellular transmissions, glutamate and ATP are released from astrocytes following an increase in $[Ca^{2+}]_i$, and both of these events are thought to be neurotoxic under ischemic conditions [2,12]. Once released, however, part of the ATP is metabolized to adenosine, reducing neuronal activity and cell death [13], complicating the roles of neurotransmitters and gliotransmitters in tissue pathophysiology. Furthermore, the exchanges of ions, ROS, apoptotic factors and nutrients throughout astrocytes via gap junctions can reduce or spread local cellular damage [2,11]. Indeed, previous studies have reported contradictory results regarding the roles of gap junctions in ischemia [14–16], potentially because of the compensatory systematic physiological changes that occur during the chronic manipulations of connexins [17]. While the roles of astrocytes in pathophysiology remains controversial, astrocytes are commonly found to respond to various physiological/pathophysiological conditions with increases in $[Ca^{2+}]_i$ [18,19]. Therefore, in this study, we characterized the pathophysiological responses of astrocytes during the acute phase of ischemia by applying two-photon $[Ca^{2+}]_i$ imaging to a pharmacologically accessible *in vitro* ischemia model, oxygen/glucose deprivation (OGD), and dissected out the cellular mechanisms as well as their roles in neuronal pathophysiology.

* Corresponding author. Fax: +81 3 3359 8889.
E-mail address: mnuriya@z2.keio.jp (M. Nuriya).

0006-291X/$ - see front matter © 2014 Elsevier Inc. All rights reserved.
http://dx.doi.org/10.1016/j.bbrc.2014.01.035

2. Materials and methods

2.1. Chemicals

Fluo-4 AM, BAPTA AM, and pluronic F-127 were purchased from Invitrogen (California, USA), while tetrodotoxin (TTX) was purchased from Abcam (Cambridge, UK). All other chemicals were purchased from Sigma Aldrich (Missouri, USA).

2.2. Brain slice preparation

All the procedures related to the care and treatment of the animals were approved by the Animal Resource Committee of the School of Medicine, Keio University. C57BL/6J mice of either sex (P14–18; SLC, Shizuoka, Japan) were anesthetized deeply with isoflurane, and cortical slices (300 μm thick) were prepared as previously described [8].The slices were loaded with 10 μM fluo-4 AM, 0.02% pluronic F-127 and 200 nM sulforhodamine 101 (SR101) in artificial cerebrospinal fluid (ACSF) containing 126 mM NaCl, 3 mM KCl, 1.14 mM NaH_2PO_4, 26 mM $NaHCO_3$, 3 mM $CaCl_2$, 1 mM $MgCl_2$, and 10 mM dextrose for 60 min at 34 °C, then transferred to normal ACSF and incubated for at least 30 min at room temperature before use in the recordings.

2.3. Imaging

Slices were transferred to a recording chamber perfused with ACSF bubbled with 95% O_2/5% CO_2 at a speed of 2.5 mL/min at 34 ± 0.5 °C and incubated for 30 min before imaging. Imaging was performed using an FV1000MPE multiphoton microscopy system (Olympus, Tokyo, Japan) equipped with a MaiTai HP femtosecond laser (Newport, California, USA) tuned to 840 nm (<15 mW under the objective lens) and a LUMPlanFL60 × WIR2 objective lens (N.A. 0.9, W.D. 2 mm; Olympus). The fluorescence signals of fluo-4 AM and SR101 were simultaneously acquired using 2-channel external photomultiplier tube detectors after the FV10MP-MG/R filter set (BA495-540HQ and BA570-625HQ; Olympus) at 512 × 512 pixels (0.41 μm/pixel). Time-lapse imaging was performed at 0.3 Hz (Kalman averaging of 2 times taken at 1.1 s/time every 3 s) for 350 frames. After 3 min of recording in normal ACSF, the solution was changed to OGD ACSF, in which the glucose had been replaced with sucrose and the solution had been bubbled with 95% N_2/5% CO_2. Images shown in Fig. 1A were smoothened for display purpose using ImageJ.

2.4. Whole cell patch clamp recording

Slices were imaged using infrared differential interference contrast. Whole cell patch clamp recordings were performed using MultiClamp 700B (Molecular Devices, California, USA). Glass pipettes (5–10 MΩ; Warner Instruments, Connecticut, USA) were filled with 100 μM Alexa Fluor 488 hydrazide (Invitrogen, California, USA) in an internal solution containing 10 mM NaCl, 10 mM KCl, 135 mM $KMeSO_4$, 2.5 mM MgATP, 0.3 mM NaGTP, and 10 mM HEPES (pH 7.3). All the recordings were performed at 34 ± 0.5 °C under the current clamp mode with zero current injection.

2.5. Data analysis

Data were analyzed using custom-written software (MATLAB; Mathworks, Massachusetts, USA) and FV10-ASW (Olympus, Tokyo, Japan). All the data are shown as the mean ± standard deviation (S.D.). To analyze the astrocytic calcium imaging data, regions of interest (ROIs) were selected at the soma based on the SR101 signals. To compensate for changes in the fluorescence intensity because of the movement of the target cells during the time-lapse imaging, the mean fluorescence intensities of fluo-4 in the ROIs were divided by those of SR101 in the corresponding ROIs: $F_t = (G_t - G_{background})/(R_t - R_{background})$, where F_t, G_t, and R_t are the adjusted fluo-4 fluorescence intensity and the original signals of fluo-4 and SR101, respectively, and $G_{background}$ and $R_{background}$ are the background signals of fluo-4 and SR101, respectively. These adjusted fluo-4 signals were used to calculate the intensity changes in fluo-4 as defined by $\Delta F_t = (F_t - F_0)/F_0$, where F_0 is the mean of F_t in the first 20 frames. Spiking events with peaks exceeding a threshold at fivefold the S.D. value calculated from the baseline recording period were considered "calcium spikes". Similarly, the onset of increases in astrocytic calcium during the second phase (see Section 3) was defined as the time immediately before the point at which ΔF_t exceeds 5 × S.D. in at least two astrocytes in the field of view relative to the time at the start of OGD exposure. When analyzing the patch clamp recordings of the neurons, the sample sizes were reduced to match those of the images by taking the average of all the data acquired during the frame scans; the onset of neuronal depolarization was defined as the time immediately before the point at which the neuronal membrane potential increased above −40 mV. To examine the synchronization of neuronal and astrocytic responses, linear fittings with a fixed intercept at 0 were performed.

All the statistical analyses were performed using Origin Pro (OriginLab, Massachusetts, USA) except for the χ^2-tests, which were performed using the custom-written software. The Mann–Whitney test was used for comparisons between the two groups, and a Bonferroni test after one-way ANOVA was used for comparisons among three groups. The asterisks in the figures indicate statistically significant differences among the groups ($P < 0.05$).

3. Results

3.1. Two-photon imaging of astrocytic $[Ca^{2+}]_i$ dynamics under OGD

To characterize the pathophysiological responses of astrocytes under ischemia, we performed two-photon calcium imaging of astrocytes in acute slices of visual cortices prepared from mice before and after exposure to OGD. To observe the changes in $[Ca^{2+}]_i$ in astrocytes, brain slices were incubated with a calcium indicator, fluo-4 AM (10 μM). As previously reported, preferential loading of the astrocytes with fluo-4 AM was achieved under this condition [20]. In all the experiments, the astrocytes were identified by the astrocyte-specific marker sulforhodamine 101 (SR101, 200 nM) [21], and imaging was performed 50–70 μm below the surface. After 3 min of baseline imaging, the perfusion solution was changed to the OGD solution. Time-lapse imaging revealed two-different types of $[Ca^{2+}]_i$ responses by the astrocytes under OGD: oscillating transients (first phase), followed by a single large increase that was often accompanied by a focus shift (second phase) (Fig. 1A and B). The focus shift, presumably caused by the swelling of the tissues, was too large to continue the $[Ca^{2+}]_i$ recording from the same set of astrocytes, and resulted in the apparent decay of the fluorescence intensity after a steep elevation during the second phase (Fig. 1A and B). These characteristic $[Ca^{2+}]_i$ responses of the astrocytes were never observed in the absence of OGD stimulation, suggesting that these $[Ca^{2+}]_i$ changes represent the pathophysiologic responses of astrocytes in the acute phase of ischemia. In the first phase, each astrocyte showed heterogeneous calcium dynamics, whereas $[Ca^{2+}]_i$ was elevated in all the astrocytes in the second phase. This simultaneous astrocytic $[Ca^{2+}]_i$ increase during the second phase is consistent with the "very early ischemic

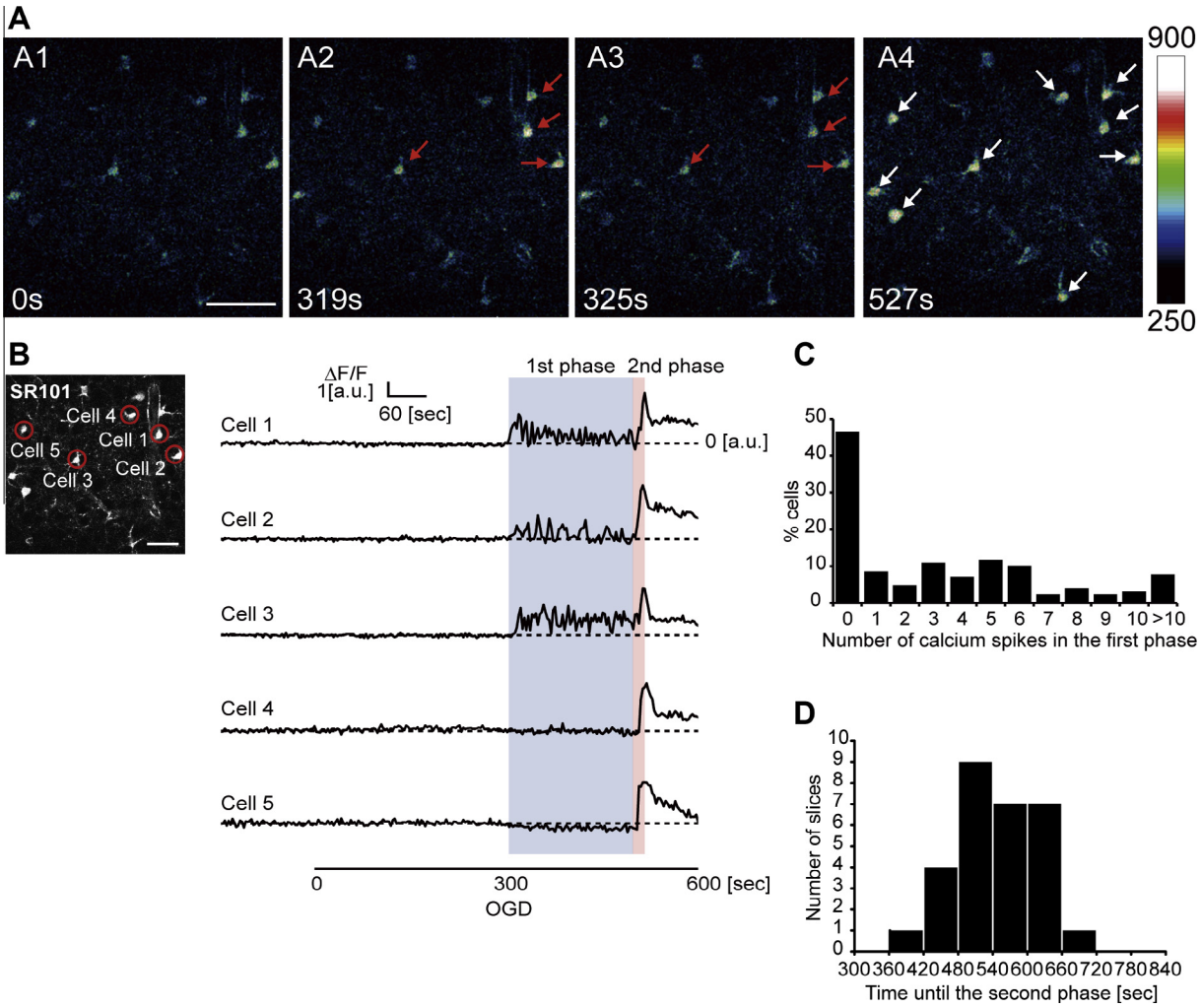

Fig. 1. Characterization of astrocytic $[Ca^{2+}]_i$ responses to OGD. (A) Images showing $[Ca^{2+}]_i$ responses in astrocytes under OGD. OGD exposure induced oscillatory $[Ca^{2+}]_i$ transients in some astrocytes (A2,3; red arrows), followed by sustained $[Ca^{2+}]_i$ increases in all the astrocytes (A4; white arrows). Scale bar, 50 μm. (B) Representative traces of astrocytic $[Ca^{2+}]_i$ changes under OGD. The upper left panel shows an SR101 image with the same focus as that shown in Fig. 1A (scale bar, 50 μm). While the astrocytic $[Ca^{2+}]_i$ dynamics were heterogeneous during the first phase (Cells 1–3 are active, Cells 4 and 5 are inactive), all the astrocytes show $[Ca^{2+}]_i$ increases nearly simultaneously during the second phase. (C) Histograms of the number of $[Ca^{2+}]_i$ spikes in each astrocyte during the first phase. (D) Histograms of the time until the onset of the second phase in each slice.

response" reported previously [3]. For quantification purposes, we assessed the astrocytic responses to OGD according to the number of spikes in each astrocyte during the first phase (Fig. 1C: active astrocytes vs. inactive astrocytes: 55.04 vs. 44.96%, $n = 129$ cells, 17 slices), and the time until the onset of the second phase in each brain slice (Fig. 1D: mean onset of the second phase: 533.4 ± 72.6 s, $n = 29$ slices).

3.2. Extracellular transmissions via mGluR5 or P2R do not contribute to the ischemic responses of astrocytes

To investigate the underlying mechanisms, we next examined the relationship between extracellular transmissions and the astrocytic calcium responses under ischemia. First, we tested the involvement of neuronal activities. However, TTX (1 μM) did not affect either the first phase (Fig. 2A: control: $n = 20$ cells, 5 slices; TTX: $n = 15$ cells, 7 slices; $P = 0.16$, χ^2-test) or the second phase (Fig. 2B: control: 546.0 ± 77.6 s, $n = 5$ slices; TTX: 598.5 ± 60.7 s, $n = 7$ slices; $P = 0.19$, Mann–Whitney Test), indicating that the astrocytic $[Ca^{2+}]_i$ responses are independent of neuronal firing under this condition. Next, we examined the roles of receptors that are known to affect astrocyte physiology. Previous reports showed that glutamate causes an increase in the $[Ca^{2+}]_i$ of astrocytes via metabolic glutamate receptor 5 (mGluR5) [10,19] and that the accumulation of extracellular glutamate is ~100 fold higher under OGD [1,2]. However, an mGluR5 antagonist, 6-methyl-2-(phenylethynyl) pyridine hydrochloride (MPEP, 50 μM), did not change the results for the first phase (Fig. 2C: control: $n = 70$ cells, 8 slices; MPEP: $n = 55$ cells, 6 slices; $P = 0.21$, χ^2-test) or the second phase (Fig. 2D: control: 561.7 ± 72.5 s, $n = 8$ slices; MPEP: 556.3 ± 124.7 s, $n = 8$ slices; $P = 0.75$, Mann–Whitney Test). Besides glutamate, accumulating evidence suggests that ATP signaling via P2 receptors (P2R) also plays key roles in the regulation of astrocytes [2,22]. However, the non-selective P2R antagonist suramin (50 μM) did not affect the first phase (Fig. 2E: control: $n = 34$ cells, 4 slices; suramin: $n = 31$cells, 5 slices; $P = 0.46$, χ^2-test) nor the second phase (Fig. 2F: control: 522.2 ± 77.9 s, $n = 4$ slices; suramin: 565.2 ± 65.1 s, $n = 5$ slices; $P = 0.56$, Mann–Whitney Test). Finally, the potential contributions of calcium-dependent releases of gliotransmitters were examined. Although the calcium chelator BAPTA AM (100 μM) almost completely blocked $[Ca^{2+}]_i$ transients during the first phase (Fig. 2G: control: $n = 19$ cells, 4 slices; BAPTA: $n = 32$ cells, 6 slices; $P < 0.05$, χ^2-test), it had no effect on the onset of the second phase (Fig. 2H: control:

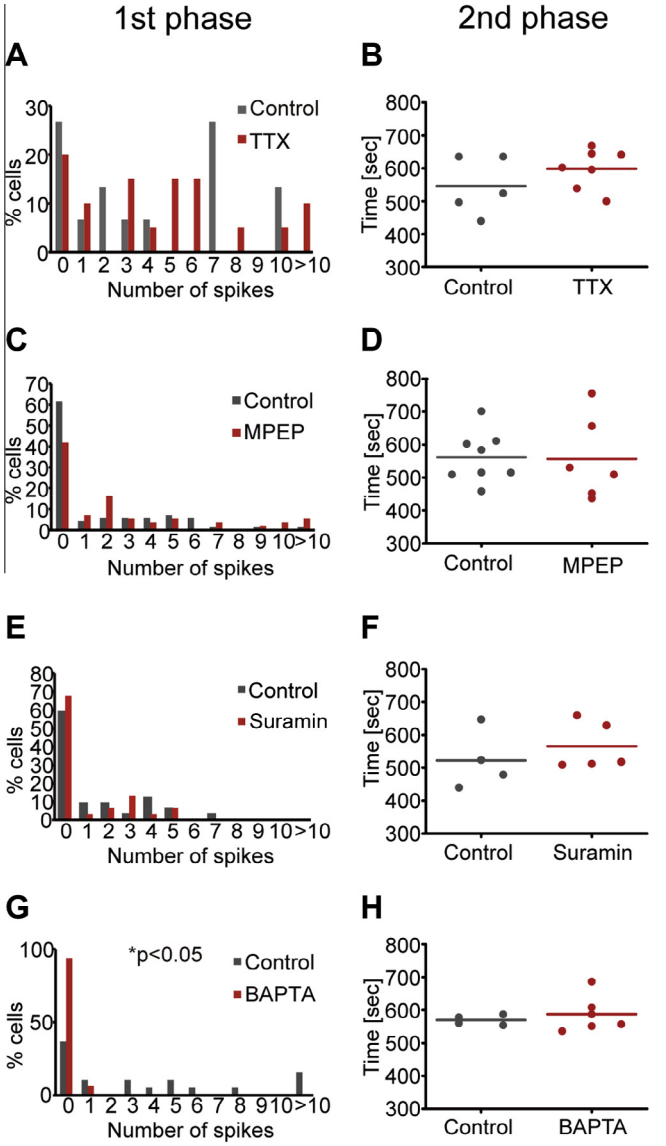

Fig. 2. Pharmacological inhibitions of extracellular transmissions do not change the astrocytic $[Ca^{2+}]_i$ responses to OGD. (A and B) $[Ca^{2+}]_i$ dynamics in astrocytes in the absence of neuronal firings. TTX (1 μM) did not have a significant effect on the number of $[Ca^{2+}]_i$ spikes during the first phase (A) or on the onset of the sustained $[Ca^{2+}]_i$ increase during the second phase (B). (C and D) $[Ca^{2+}]_i$ dynamics in astrocytes in the presence of an mGluR5 antagonist. MPEP (50 μM) did not have a significant effect on the first phase (C) or on the second phase (D). (E and F) $[Ca^{2+}]_i$ dynamics in astrocytes in the presence of a P2 receptor antagonist. Suramin (50 μM) did not have a significant effect on the first phase (E) or on the second phase (F). (G and H) $[Ca^{2+}]_i$ dynamics in astrocytes in the presence of a calcium chelator. BAPTA AM (100 μM) totally blocked the $[Ca^{2+}]_i$ dynamics during the first phase (G) but did not have a significant effect on the onset of the sustained $[Ca^{2+}]_i$ increase during the second phase (H).

569.6 ± 13.4 s, $n = 4$ slices; BAPTA: 587.4 ± 59.2 s, $n = 6$ slices; $P = 1$, Mann–Whitney Test). Persistence of the $[Ca^{2+}]_i$ rise in the second phase under this condition suggests that the high-magnitude and long-lasting calcium influx into the cytosol (Fig. 1B) exceed the buffering capacity of the intracellularly-loaded BAPTA. Therefore, to elucidate the source of calcium ions in the second phase, the same experiments were performed under more robust, tissue-wide manipulations of calcium ions. We found that perturbations of calcium influxes from either the extracellular space or the endoplasmic reticulum partially inhibited the emergence of the second phase, suggesting that calcium ions enter the cytoplasm from both sources (Supplementary materials), consistent with the previous report [3]. Taken together, these results suggest that the activations of mGluR5 and P2R, both of which have been suggested to evoke astrocytic $[Ca^{2+}]_i$ dynamics, do not contribute to the pathophysiology of astrocytes under OGD.

3.3. Inhibition of gap junctional coupling advances the appearance of ischemic responses of astrocytes

In addition to the extracellular transmissions, astrocytes communicate with each other through gap junctions. Therefore, we next examined whether gap junctional coupling contributed to the ischemic responses of astrocytes. In the presence of a gap junction blocker, carbenoxolone (CBX, 50 μM), while no change was seen during the first phase (Fig. 3A: control: $n = 41$ cells, 7 slices; CBX: $n = 62$ cells, 8 slices; $P = 0.49$, χ^2-test), the onset of the second phase was significantly advanced (Fig. 3B). The specificity of the pharmacological blockade of the gap junctions was further confirmed by another gap junction blocker, 18 β-glycyrrhetinic acid (β-GA, 50 μM) (Fig. 3B: control: 562.2 ± 88.1 s, $n = 13$ slices; CBX: 447.9 ± 58.3 s, $n = 9$ slices; β-GA: 451.5 ± 69.6 s, $n = 6$ slices, $P < 0.05$, Bonferroni test after one-way ANOVA). Besides gap junctions, these pharmacological manipulations are likely to block hemichannels formed by connexins and pannexins [23]. To evaluate the potential involvement of hemichannels in the formation of astrocytic responses to OGD, we applied lantunum (La^{3+}, 100 μM), which blocks both connexin and pannexin hemichannels, and a lower concentration of CBX (5 μM), which preferentially affects high affinity pannexins while having minimal effects on low affinity connexins [23]. However, neither La^{3+} nor a lower concentration of CBX affects the onset of second phase (Fig. 3C: control: 542.6 ± 61.7 s, $n = 11$ slices; La^{3+}: 544.8 ± 64.6 s, $n = 6$ slices; 5 μM CBX: 571.4 ± 106.8 s, $n = 7$ slices; $P > 0.05$, Bonferroni test after one-way ANOVA), indicating that gap junctions but not hemichannels delay the onset of the second phase.

3.4. Manipulations of astrocytic gap junctions affect the pathophysiological responses of neurons

Finally, to investigate the potential roles of astrocytes in neuronal pathophysiology under ischemia, we recorded the membrane

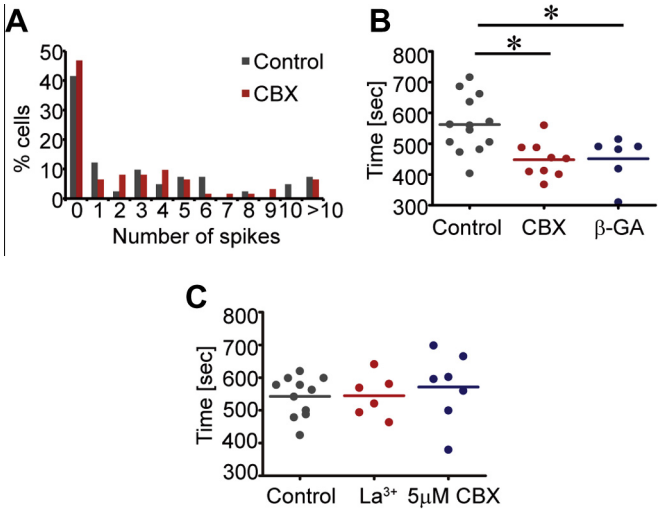

Fig. 3. $[Ca^{2+}]_i$ dynamics in astrocytes in the presence of gap junction blockers. (A and B) CBX (50 μM) did not affect the $[Ca^{2+}]_i$ dynamics of astrocytes during the first phase (A) but significantly advanced the onset of the sustained $[Ca^{2+}]_i$ increase during the second phase (B). Similarly, the second phase appeared more quickly in the presence of another gap junction blocker, β-GA (50 μM) (B). $^*P < 0.05$. (C) Neither La^{3+} (100 μM) nor CBX at the lower concentration (5 μM) affected the onset of the second phase.

potential of neurons using whole cell patch clamp recordings, together with the astrocytic $[Ca^{2+}]_i$ dynamics. As reported previously, we observed a sudden and large irreversible depolarization under OGD, known as anoxic depolarization that is the hallmark of ischemic neuronal responses causing glutamate release, cell swelling, and neuronal cell death (Fig. 4A) [24,25]. A comparison between the astrocytic $[Ca^{2+}]_i$ and neuronal membrane potential responses revealed that the onsets of the second phase of the astrocytic $[Ca^{2+}]_i$ dynamics were tightly synchronized with the appearance of the anoxic depolarization of the neurons ($y = 1.005\ x$, $R^2 = 0.998$, $n = 6$ slices), suggesting that the second phase of the astrocytic $[Ca^{2+}]_i$ represents the onset of tissue damage in response to ischemic insults (Fig. 4A and C). Furthermore, this result also suggests the existence of functional interactions between neurons and astrocytes upon exposure to OGD and raises the possibility that astrocytes take a leading role in determining the progression of the pathophysiology of the brain tissue, including neurons. To test this hypothesis, we examined the effect of a gap junction blocker on the neuronal responses under OGD. Indeed, the pharmacological blockade of the gap junction advanced the initiation of neuronal depolarization under OGD (control: 534.9 ± 64.7 s, $n = 6$ slices; CBX: 450.7 ± 33.9 s, $n = 6$ slices; $P < 0.05$, Mann–Whitney Test) as well as the onset of an astrocytic $[Ca^{2+}]_i$ elevation during the second phase (control: 537.4 ± 67.3 s, $n = 6$ slices; CBX: 451.2 ± 30.5 s, $n = 6$ slices; $P < 0.05$, Mann–Whitney Test), maintaining the synchronization of anoxic depolarization and the astrocytic responses ($y = 1.001\ x$, $R^2 = 0.975$, $n = 6$ slices) (Fig. 4B and C). Taken together, these results suggest that astrocytic gap junctional coupling delays the appearance of pathophysiological responses in neurons as well as in astrocytes themselves.

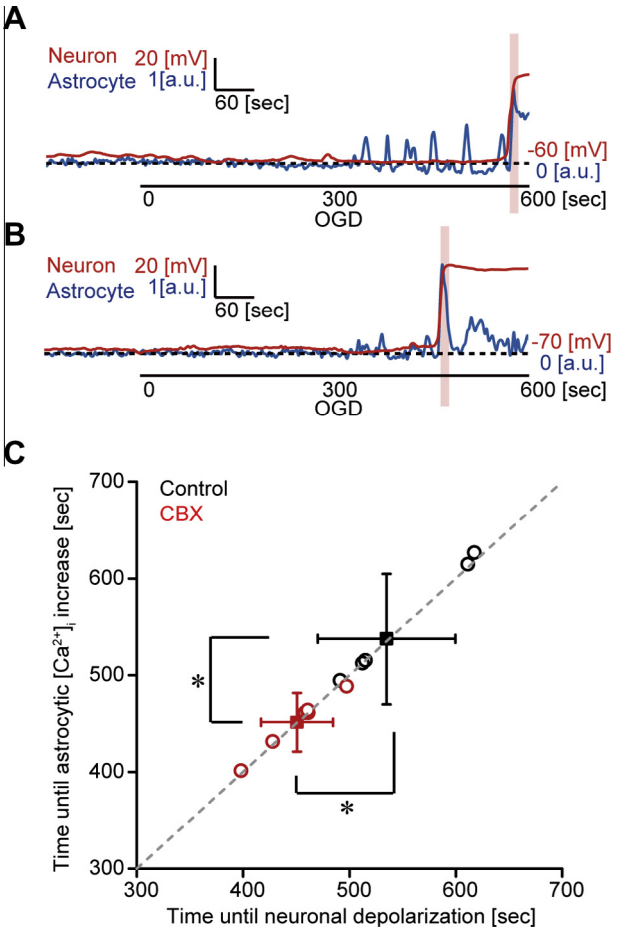

Fig. 4. Effect of gap junctional blockade on the neuronal responses to OGD. (A and B) Representative traces of astrocytic $[Ca^{2+}]_i$ changes (blue line) and neuronal membrane potential changes (red line) in the control (A) or in the presence of CBX (B). (C) The onset of the second phase of $[Ca^{2+}]_i$ changes in astrocytes and the appearance of neuronal anoxic depolarization are synchronized. Each point indicates the onset of the second phase of $[Ca^{2+}]_i$ changes in astrocytes and the appearance of neuronal anoxic depolarization in a slice (control: black circle, CBX: red circle). Filled squares and whiskers represent means and SDs, respectively. The linear fit of the data indicates the synchronization of these responses. The dotted line indicates $y = x$, and $^*P < 0.05$.

4. Discussion

In this study, we characterized the astrocytic $[Ca^{2+}]_i$ responses in cortical slices under OGD and revealed that astrocytes protect neurons against ischemic insults through gap junctional couplings.

Our analysis using high-resolution two-photon time-lapse imaging revealed that about half of the astrocytes show oscillatory $[Ca^{2+}]_i$ spikes during the first phase under OGD, in addition to the universal sustained $[Ca^{2+}]_i$ increases (Fig. 1), as reported previously [3]. In the first phase, the astrocytic $[Ca^{2+}]_i$ responses varied among the cells (Fig. 1A–C), suggesting that astrocytes sense local ischemic changes individually, consistent with the concept of non-overlapping local domains covered by individual astrocytes [26]. Nevertheless, while the intracellularly loaded calcium chelator BAPTA almost completely blocked the calcium spikes of astrocytes during the first phase, it did not affect the onset of the second phase, suggesting that the second phase may be independent of the astrocytic calcium activities during the first phase (Fig. 2G and H). Together, our results suggest that astrocytes sense ischemic insults even before neurons, but their $[Ca^{2+}]_i$ changes may not play active roles against severe ischemic damages, calling for further investigations of the still-debated nature of calcium responses in astrocytes in brain physiology/pathophysiology [18,19].

As for the second phase, pharmacological inhibitions showed that the blockade of gap junction coupling but not hemichannels hastened the onset of this phase (Fig. 3). While the involvement of neuronal gap junctions cannot be completely ruled out in our system, their contributions to the observed effects appear to be unlikely because (1) the expression levels of gap junction proteins in neurons are very low, compared with in astrocytes [27], and (2) our results indicated that the neuronal activities play a minimal role, if any, in the progression of the acute phase of ischemia (Fig. 2A and B). Interestingly, in sharp contrast to the first phase, the onset of the second phase is synchronized among all astrocytes (Fig. 1), consistent with the involvement of the gap junctional network during this phase (Fig. 3). Furthermore, this astrocytic response is accompanied by anoxic neuronal depolarization (Fig. 4), the hallmark of neuronal cell damage under ischemic conditions [24]. Taken together, these results indicate that the gap junction-mediated astrocytic syncytium plays a protective role against tissue-wide damages during the acute phase of ischemia, with their capacity to buffer local damages through a global network.

Acknowledgments

The authors declare no conflicts of interests. This work was supported by MEXT Japan (KAKENHI # 23657106 to M.N.), the Sumitomo Foundation (M.N.), the Takeda Science Foundation (M.N.), the Japan New Energy and Industrial Technology Development Organization (NEDO, to M.Y.), the Keio Gijuku Graduate School Doctoral Student Grant-in-Aid Program (T.S.), and the Strategic Japanese-Swedish Cooperative Program from the Japan Science and Technology Agency (M.Y.). We would like to thank Olympus Corporation for providing technical assistance.

Appendix A. Supplementary data

Supplementary data associated with this article can be found, in the online version, at http://dx.doi.org/10.1016/j.bbrc.2014.01.035.

References

[1] P. Lipton, Ischemic cell death in brain neurons, Physiol. Rev. 79 (1999) 1431–1568.
[2] D.J. Rossi, J.D. Brady, C. Mohr, Astrocyte metabolism and signaling during brain ischemia, Nat. Neurosci. 10 (2007) 1377–1386.
[3] S. Duffy, B.A. MacVicar, In vitro ischemia promotes calcium influx and intracellular calcium release in hippocampal astrocytes, J. Neurosci. 16 (1996) 71–81.
[4] Q.P. Dong, J.Q. He, Z. Chai, Astrocytic Ca(2+) waves mediate activation of extrasynaptic NMDA receptors in hippocampal neurons to aggravate brain damage during ischemia, Neurobiol. Dis. 58 (2013) 68–75.
[5] S. Ding, T. Wang, W. Cui, et al., Photothrombosis ischemia stimulates a sustained astrocytic Ca2+ signaling in vivo, Glia 57 (2009) 767–776.
[6] G. Xu, W. Wang, H.K. Kimelberg, et al., Electrical coupling of astrocytes in rat hippocampal slices under physiological and simulated ischemic conditions, Glia 58 (2010) 481–493.
[7] W.C. Risher, R.D. Andrew, S.A. Kirov, Real-time passive volume responses of astrocytes to acute osmotic and ischemic stress in cortical slices and in vivo revealed by two-photon microscopy, Glia 57 (2009) 207–221.
[8] M. Nuriya, T. Shinotsuka, M. Yasui, Diffusion properties of molecules at the blood–brain interface: potential contributions of astrocyte endfeet to diffusion barrier functions, Cereb. Cortex 23 (2013) 2118–2126.
[9] M. Nedergaard, U. Dirnagl, Role of glial cells in cerebral ischemia, Glia 50 (2005) 281–286.
[10] A. Volterra, J. Meldolesi, Astrocytes, from brain glue to communication elements: the revolution continues, Nat. Rev. Neurosci. 6 (2005) 626–640.
[11] C. Giaume, A. Koulakoff, L. Roux, et al., Astroglial networks: a step further in neuroglial and gliovascular interactions, Nat. Rev. Neurosci. 11 (2010) 87–99.
[12] T. Takano, N. Oberheim, M.L. Cotrina, et al., Astrocytes and ischemic injury, Stroke 40 (2009) S8–12.
[13] J.H. Lin, N. Lou, N. Kang, et al., A central role of connexin 43 in hypoxic preconditioning, J. Neurosci. 28 (2008) 681–695.
[14] T. Nakase, S. Fushiki, C.C. Naus, Astrocytic gap junctions composed of connexin 43 reduce apoptotic neuronal damage in cerebral ischemia, Stroke 34 (2003) 1987–1993.
[15] M.V. Frantseva, L. Kokarovtseva, J.L. Perez Velazquez, Ischemia-induced brain damage depends on specific gap-junctional coupling, J. Cereb. Blood Flow Metab. 22 (2002) 453–462.
[16] J.H. Lin, H. Weigel, M.L. Cotrina, et al., Gap-junction-mediated propagation and amplification of cell injury, Nat. Neurosci. 1 (1998) 494–500.
[17] P. Ezan, P. Andre, S. Cisternino, et al., Deletion of astroglial connexins weakens the blood-brain barrier, J. Cereb. Blood Flow Metab. 32 (2012) 1457–1467.
[18] M. Nedergaard, J.J. Rodriguez, A. Verkhratsky, Glial calcium and diseases of the nervous system, Cell Calcium 47 (2010) 140–149.
[19] C. Agulhon, J. Petravicz, A.B. McMullen, et al., What is the role of astrocyte calcium in neurophysiology?, Neuron 59 (2008) 932–946
[20] K.E. Poskanzer, R. Yuste, Astrocytic regulation of cortical UP states, Proc. Nat. Acad. Sci. 108 (2011) 18453–18458.
[21] A. Nimmerjahn, F. Kirchhoff, J.N. Kerr, et al., Sulforhodamine 101 as a specific marker of astroglia in the neocortex in vivo, Nat. Methods 1 (2004) 31–37.
[22] N.B. Hamilton, D. Attwell, Do astrocytes really exocytose neurotransmitters?, Nat Rev. Neurosci. 11 (2010) 227–238.
[23] C. Giaume, M. Theis, Pharmacological and genetic approaches to study connexin-mediated channels in glial cells of the central nervous system, Brain Res. Rev. 63 (2010) 160–176.
[24] E. Tanaka, S. Yamamoto, Y. Kudo, et al., Mechanisms underlying the rapid depolarization produced by deprivation of oxygen and glucose in rat hippocampal CA1 neurons in vitro, J. Neurophysiol. 78 (1997) 891–902.
[25] D.J. Rossi, T. Oshima, D. Attwell, Glutamate release in severe brain ischaemia is mainly by reversed uptake, Nature 403 (2000) 316–321.
[26] G.C. Petzold, V.N. Murthy, Role of astrocytes in neurovascular coupling, Neuron 71 (2011) 782–797.
[27] J.E. Rash, T. Yasumura, F.E. Dudek, et al., Cell-specific expression of connexins and evidence of restricted gap junctional coupling between glial cells and between neurons, J. Neurosci. 21 (2001) 1983–2000.